

Late Energy Injection and Cosmological Constraints in Axino Dark Matter Scenarios

Ayres Freitas,^{1,*} Frank Daniel Steffen,^{2,†} Nurhana Tajuddin,^{3,‡} and Daniel Wyler^{3,§}

¹*Department of Physics and Astronomy, University of Pittsburgh, PA 15260, USA*

²*Max-Planck-Institut für Physik, Föhringer Ring 6, D-80805 Munich, Germany*

³*Institut für Theoretische Physik, Universität Zürich,
Winterthurerstrasse 190, CH-8057 Zürich, Switzerland*

Taking into account effects of late energy injection, we examine big bang nucleosynthesis (BBN) constraints on axino dark matter scenarios with long-lived charged sleptons. We calculate 4-body slepton decays into the axino, a lepton, and a quark-antiquark pair since they govern late hadronic energy injection and associated BBN constraints. For supersymmetric hadronic axion models, we present the obtained hadronic BBN constraints and show that they can be more restrictive than the ones associated with catalyzed BBN via slepton-bound-state formation. From the BBN constraints on hadronic and electromagnetic energy release, we find new upper limits on the Peccei–Quinn scale.

PACS numbers: 98.80.Cq, 95.35.+d, 12.60.Jv, 95.30.Cq

I. INTRODUCTION

It is widely believed that the Standard Model of particle physics is not complete and that new physics is required for a compelling theoretical description of nature. The Large Hadron Collider (LHC) may give us a first opportunity to test models of new physics directly.

In addition to collider experiments, the early Universe offers many ways to probe new physics. In particular, the observed dark matter density and the framework of big bang nucleosynthesis (BBN) impose valuable restrictions on the parameters of new physics models.

Supersymmetry (SUSY) and the Peccei–Quinn (PQ) symmetry are particularly well-motivated extensions of the Standard Model each of which comes with a compelling dark matter candidate. If both of these extensions are realized simultaneously, significant contributions to the cold dark matter density Ω_{dm} can reside in the axion and/or the lightest supersymmetric particle (LSP).

An attractive realization of this scenario with conserved R-parity has the axino \tilde{a} —the fermionic partner of the axion—as the LSP and a charged slepton \tilde{l}_1 as the next-to-lightest supersymmetric particle (NLSP). In fact, the axino is an extremely weakly interacting particle and a promising dark matter candidate beyond the minimal supersymmetric Standard Model (MSSM) [1, 2, 3, 4, 5, 6, 7, 8]. Since the axino LSP allows for a long-lived charged slepton—such as the lighter stau $\tilde{\tau}_1$ —which should be easy to discover at the LHC, those scenarios are appealing not only from a theoretical point of view but also from a phenomenological one.

The requirement of avoiding overclosure of the Universe from an overly efficient production of axino dark

matter allows one to derive upper limits on the reheating temperature [3, 5, 7, 8, 9, 10, 11]. In our recent Letter [8], we have shown how those constraints become more restrictive in the above scenarios once catalyzed BBN (CBBN) and the associated production of primordial lithium-6 and beryllium-9 [12, 13, 14] are considered. Moreover, while axion physics provides us with a lower limit [15, 16, 17]

$$f_a \gtrsim 6 \times 10^8 \text{ GeV}, \quad (1)$$

we found that CBBN also imposes upper limits on f_a that depend on the slepton mass [8].

In this Letter we further develop the BBN constraints on axino LSP scenarios with long-lived charged sleptons by considering hadronic and electromagnetic energy injection. If the \tilde{l}_1 is relatively long-lived, decay modes with hadrons in the final state can affect BBN and are thus strongly restricted. We analyze the most important contribution of this kind: the hadronic 4-body decay of \tilde{l}_1 into the associated lepton, the axino, and a quark-antiquark pair. We also include the electromagnetic energy injection, which is derived from the 2-body decay of the \tilde{l}_1 into the the associated lepton and the axino. In fact, the BBN constraints on hadronic and electromagnetic energy release allow us to derive new upper limits on f_a which appear in addition to those imposed by CBBN.

II. PARTICLE PHYSICS SETTING

We consider SUSY hadronic (or KSVZ [18, 19]) axion models [20] in which the interaction of the axion multiplet Φ with the heavy KSVZ quark multiplets Q_1 and Q_2 is described by the superpotential

$$W_{\text{PQ}} = y\Phi Q_1 Q_2 \quad (2)$$

with the Yukawa coupling y and the quantum numbers given in Table I. With the 2-component fields listed in

*Electronic address: afreitas@pitt.edu

†Electronic address: steffen@mppmu.mpg.de

‡Electronic address: nurhana@physik.uzh.ch

§Electronic address: wyler@physik.unizh.ch

TABLE I: Quantum numbers of the axion multiplet Φ and the heavy KSVZ quark multiplets $Q_{1,2}$ considered in this work.

chiral multiplet	$U(1)_{PQ}$	$(SU(3)_c, SU(2)_L)_Y$
$\Phi = \phi + \sqrt{2}\chi\theta + F_\Phi\theta\theta$	+1	$(\mathbf{1}, \mathbf{1})_0$
$Q_1 = \tilde{Q}_1 + \sqrt{2}q_1\theta + F_1\theta\theta$	-1/2	$(\mathbf{3}, \mathbf{1})_{+e_Q}$
$Q_2 = \tilde{Q}_2 + \sqrt{2}q_2\theta + F_2\theta\theta$	-1/2	$(\mathbf{3}^*, \mathbf{1})_{-e_Q}$

that table, the axino and the heavy KSVZ quarks are described by the respective 4-component fields,

$$\tilde{a} = \begin{pmatrix} \chi \\ \bar{\chi} \end{pmatrix} \quad \text{and} \quad Q = \begin{pmatrix} q_1 \\ \bar{q}_2 \end{pmatrix}. \quad (3)$$

For the heavy KSVZ (s)quark masses, we use the SUSY limit $M_{\tilde{Q}_{1,2}} = M_Q = y\langle\phi\rangle = yf_a/\sqrt{2}$ with both y and $\langle\phi\rangle$ taken to be real by field redefinitions.¹ Accordingly, the phenomenological constraint (1) implies, for $y = \mathcal{O}(1)$, a large mass hierarchy between the KSVZ fields and the weak and the soft SUSY mass scales,

$$M_{Q/\tilde{Q}_{1,2}} \gg M_Z, m_{\text{SUSY}}. \quad (4)$$

While our study can easily be generalized, we focus on the case in which the NLSP is a purely right-chiral lighter stau, $\tilde{\tau}_1 = \tilde{\tau}_R$, which is a good approximation at least for small $\tan\beta$. Its coupling to neutralinos is then dominated by the bino coupling. For further simplicity, we assume that mixing in the neutralino sector is such that one of the neutralino states is an (almost) pure bino. In fact, our cosmological considerations rely on a spectrum in which that state is the lightest neutralino, $\tilde{\chi}_1^0 = \tilde{B}$, while our results for the $\tilde{\tau}_R$ decays are not restricted to this case. We treat the axino mass $m_{\tilde{a}}$ as a free parameter which is bounded from above by the stau NLSP mass $m_{\tilde{\tau}}$.

In the considered R-parity conserving setting, the lifetime of the $\tilde{\tau}_R$ NLSP is governed by the decay $\tilde{\tau}_R \rightarrow \tau\tilde{a}$,

$$\tau_{\tilde{\tau}} = 1/\Gamma_{\text{tot}}^{\tilde{\tau}_R} \approx 1/\Gamma(\tilde{\tau}_R \rightarrow \tau\tilde{a}), \quad (5)$$

where the dominant contributions to the partial width $\Gamma(\tilde{\tau}_R \rightarrow \tau\tilde{a})$ occur at the two-loop level.² Using a heavy mass expansion in powers of $1/f_a$ [21], we have recently calculated the leading term that governs (5) [8].

¹ To avoid ambiguities related to the f_a definition, $f_a = \sqrt{2}\langle\phi\rangle$, the effective axion interactions obtained from (2) after integrating out the heavy KSVZ fields are given in Sect. 3 of Ref. [8].

² As noted in [4, 8, 21, 22], the 3-body decay $\tilde{\tau}_R \rightarrow \tau\tilde{a}\gamma$ occurs already at the 1-loop level, but for most of the phase space is subdominant. Moreover, compared to the 3-body decay, the 4-body decay modes $\tilde{\tau}_R \rightarrow \tau\tilde{a}\gamma\gamma$, $\tau\tilde{a}^{++}l^-$, $\tau\tilde{a}q\bar{q}$ are suppressed by an additional factor of α ; cf. Fig. 1 below.

III. ENERGY RELEASE IN STAU DECAYS

Decays of the $\tilde{\tau}_R$ NLSP into the \tilde{a} LSP are associated with the emission of Standard Model particles. If injected at cosmic times $t \gtrsim 100$ s, i.e., during or after BBN, those particles can reprocess the primordial light elements significantly via hadrodissociation and/or photodissociation. At earlier times, energetic particles are stopped efficiently through electromagnetic interactions so that hadrodissociation/photodissociation becomes an important issue only for $\tau_{\tilde{\tau}} \gtrsim 100$ s; see Ref. [23, 24, 25] and references therein.³

In this section, we explore the (average) electromagnetic/hadronic energy emitted in a single $\tilde{\tau}_R$ decay: $\epsilon_{\text{em/had}}$. We will use this quantity below to investigate whether successful BBN predictions are preserved.

The electromagnetic energy release ϵ_{em} is governed by the tau emitted in the main decay channel $\tilde{\tau}_R \rightarrow \tau\tilde{a}$ with an energy $E_\tau = (m_{\tilde{\tau}}^2 - m_{\tilde{a}}^2 + m_\tau^2)/(2m_{\tilde{\tau}})$ in the rest frame of the $\tilde{\tau}_R$. For stau decays at cosmic times $t \gtrsim 100$ s, the emitted tau decays before interacting electromagnetically. As each τ decays into at least one ν , which does not interact electromagnetically, only a fraction of E_τ contributes [28, 29]. We use the conservative estimate

$$\epsilon_{\text{em}} = 0.3 E_\tau = 0.3 \frac{m_{\tilde{\tau}}^2 - m_{\tilde{a}}^2 + m_\tau^2}{2m_{\tilde{\tau}}} \quad (6)$$

to avoid that the electromagnetic BBN constraints presented in Sect. VI are overly restrictive.

The hadronic energy release ϵ_{had} is governed by the quark–antiquark pair emitted in the 4-body decay $\tilde{\tau}_R \rightarrow \tau\tilde{a}q\bar{q}$. Mesons from decays of the τ 's emitted in the main decay channel $\tilde{\tau}_R \rightarrow \tilde{a}\tau$ typically decay before interacting hadronically [23]. In fact, since mesons typically decay before interacting with the background nuclei, only the nucleons originating from hadronization of the $q\bar{q}$ pair need to be taken into account for $\tau_{\tilde{\tau}} \gtrsim 100$ s. We thus consider only $q\bar{q}$ pairs with an invariant mass $m_{q\bar{q}}$ above the mass of a pair of nucleons, $m_{q\bar{q}} > m_{q\bar{q}}^{\text{cut}} = 2$ GeV, when calculating

$$\epsilon_{\text{had}} \equiv \frac{1}{\Gamma_{\text{tot}}^{\tilde{\tau}_R}} \int_{m_{q\bar{q}}^{\text{cut}}}^{m_{\tilde{\tau}} - m_{\tilde{a}} - m_\tau} dm_{q\bar{q}} m_{q\bar{q}} \frac{d\Gamma(\tilde{\tau}_R \rightarrow \tau\tilde{a}q\bar{q})}{dm_{q\bar{q}}}. \quad (7)$$

According to the value of $m_{q\bar{q}}$, all quark flavors that can occur in the final state are taken into account in the differential decay rate $d\Gamma(\tilde{\tau}_R \rightarrow \tau\tilde{a}q\bar{q})/dm_{q\bar{q}}$.

The Feynman diagrams of the dominant contributions to the 4-body decay $\tilde{\tau}_R \rightarrow \tau\tilde{a}q\bar{q}$ are illustrated in Fig. 1, where the blobs represent heavy KSVZ (s)quark loops; cf. Fig. 2 of Ref. [8]. As in the calculation of the 2-body

³ The presence of additional slow hadrons can also affect BBN through proton–neutron interconversion processes [26]. The associated limits are not considered since they are typically milder; cf. [27] for a discussion in \tilde{G} LSP scenarios with a stau NLSP.

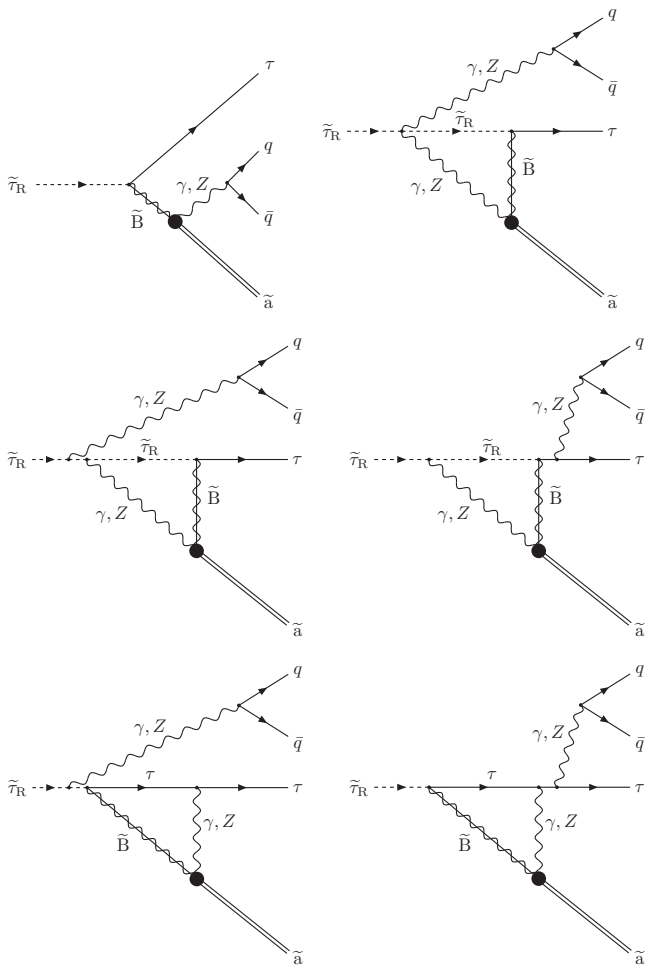


FIG. 1: Feynman diagrams of the dominant contributions to the stau NLSP decay $\tilde{\tau}_R \rightarrow \tau \tilde{a} q \bar{q}$ in a SUSY hadronic axion model. Here the lightest neutralino is assumed to be a pure bino $\tilde{\chi}_1^0 = \tilde{B}$ and the tau mass is neglected. The blob represents the loops involving the heavy KSVZ (s)quark fields with quantum numbers given in Table I; cf. Fig. 2 in Ref. [8].

decay [8], we work in the limit $m_\tau \rightarrow 0$ which is justified since $m_\tau \ll m_{\tilde{\tau}}$. Taking advantage of (4), we use again the method of heavy mass expansion to expand in heavy (s)quark masses, keeping only the leading terms $\propto 1/f_a$ in the calculation of the decay amplitude.

Although the decay first occurs at the 1-loop level, the shown 2-loop diagrams are also important as their contribution to the amplitude is enhanced by large logarithms $\ln(y f_a / \sqrt{2} m_{\tilde{\tau}}) \simeq 20$, e.g., for $m_{\tilde{\tau}}/y = 100$ GeV and $f_a = 10^{11}$ GeV. This enhancement largely compensates for the loop suppression factor governed by the fine-structure constant $\alpha = e^2/(4\pi)$. Therefore, only the leading logarithmic term of the 2-loop contribution is kept.

There are more diagrams at the 2-loop level than those shown as part of Fig. 1. One group has a γ, Z line that splits into the $q\bar{q}$ pair after originating either from the $\tilde{\tau}_R$ or τ in the loop or from one of the heavy (s)quarks in the blob. However contributions of these diagrams are

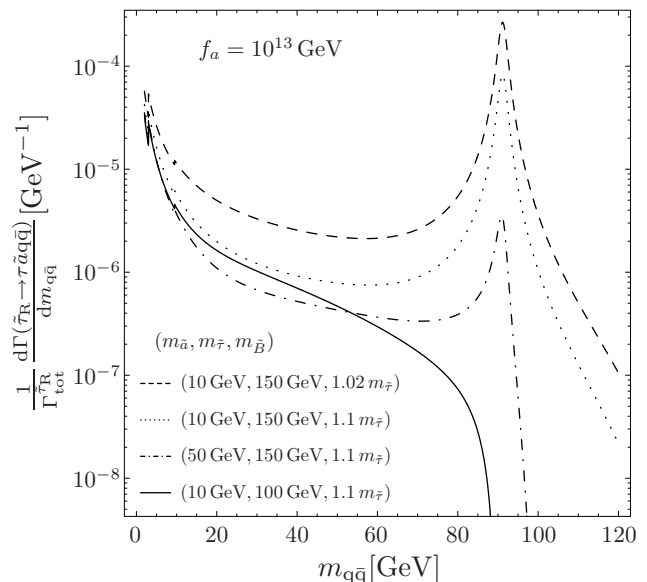


FIG. 2: Energy spectrum of the quark–antiquark pair emitted in the four-body decay $\tilde{\tau}_R \rightarrow \tau \tilde{a} q \bar{q}$ with an invariant mass $m_{q\bar{q}}$, normalized to the total decay rate $\Gamma_{\text{tot}}^{\tilde{\tau}_R} \approx \Gamma(\tilde{\tau}_R \rightarrow \tau \tilde{a})$. The shown quantity is independent of e_Q . The other parameters are set to $f_a = 10^{13}$ GeV and $y = 1$.

canceling or not enhanced by large logarithms and therefore neglected in our calculation. Similarly, there are diagrams with gluons (more than one because of color conservation) emitted by the heavy (s)quarks in the blob at higher order in the strong coupling, turning into nucleons. These are also highly suppressed and thus neglected.

In Fig. 2, our results for the differential decay rate $d\Gamma(\tilde{\tau}_R \rightarrow \tau \tilde{a} q \bar{q})/dm_{q\bar{q}}$ normalized to the total decay rate $\Gamma_{\text{tot}}^{\tilde{\tau}_R}$ are shown for $(m_{\tilde{a}}, m_{\tilde{\tau}}, m_{\tilde{B}})$ combinations of (10 GeV, 100 GeV, $1.1 m_{\tilde{\tau}}$), (50 GeV, 150 GeV, $1.1 m_{\tilde{\tau}}$), (10 GeV, 150 GeV, $1.1 m_{\tilde{\tau}}$), and (10 GeV, 150 GeV, $1.02 m_{\tilde{\tau}}$) by the solid, dash-dotted, dotted, and dashed curves, respectively. The shown quantity is independent of e_Q . The other parameters are set to $f_a = 10^{13}$ GeV and $y = 1$. The kinks at $m_{q\bar{q}} \simeq 3$ GeV and 10 GeV mark the respective thresholds for the production of $c\bar{c}$ and $b\bar{b}$ pairs. Moreover, one can see the contribution of the Z -boson resonance at $m_{q\bar{q}} = M_Z$, which is present for $\Delta m \equiv m_{\tilde{\tau}} - m_{\tilde{a}} - m_\tau > M_Z$. As part of the integrand in (7), the shown energy spectrum of the emitted $q\bar{q}$ pair is the crucial quantity in the calculation of ϵ_{had} . Based on the numerical results from the integration in (7), we obtain the hadronic BBN constraints presented in Sects. V and VI. We note that a more precise calculation of the constraints would require, in addition to $d\Gamma(\tilde{\tau}_R \rightarrow \tau \tilde{a} q \bar{q})/dm_{q\bar{q}}$, a treatment of the fragmentation of the quarks into hadrons and of the propagation of the resulting hadron spectra when computing the abundances of primordial light elements; cf. [23, 25, 30, 31].

IV. COSMOLOGICAL SETTING

In addition to $\tau_{\tilde{\tau}}$ and $\epsilon_{\text{em/had}}$, the stau NLSP yield prior to decay, $Y_{\tilde{\tau}} \equiv n_{\tilde{\tau}_R}/s$, is another quantity that is crucial for our study of cosmological constraints. Here s denotes the entropy density and $n_{\tilde{\tau}_R} = n_{\tilde{\tau}_R^+} + n_{\tilde{\tau}_R^-} = 2n_{\tilde{\tau}_R^-}$ the total $\tilde{\tau}_R$ number density prior to decay for an equal number of positively and negatively charged $\tilde{\tau}_R$ s. In contrast to $\tau_{\tilde{\tau}}$ and $\epsilon_{\text{em/had}}$, $Y_{\tilde{\tau}}$ depends on the thermal history of the early Universe. In this Letter we assume a standard thermal history with a reheating temperature after inflation in the range: $T_{\text{dec}}^{\tilde{\tau}_R} < T_R < f_a$, where $T_{\text{dec}}^{\tilde{\tau}_R} \sim m_{\tilde{\tau}}/25$ is the temperature at which the $\tilde{\tau}_R$ NLSP species decouples from the primordial plasma. This has a number of implications:

- (i) Focussing on a standard thermal history, we assume that effects of the saxion—the bosonic partner of the axino that appears in addition to the axion—are negligible. For a non-standard thermal history associated with significant late entropy production in saxion decays [32, 33, 34, 35], cosmological constraints [10] including those considered in this work can be affected depending on the saxion properties.
- (ii) For $T_R < f_a$, no PQ symmetry restoration takes place after inflation. In fact, we assume that the PQ symmetry was broken before inflation and not restored afterwards. For large f_a such that axions are never in thermal equilibrium with the primordial plasma, the relic axion density Ω_a is then governed by the initial misalignment angle Θ_i of the axion field with respect to the CP-conserving position; cf. [16, 17] and references therein. This allows us to keep the presented constraints conservative by assuming $\Omega_a \ll \Omega_{\text{dm}}$ which is possible even for f_a above 10^{14} GeV since Θ_i can be sufficiently small.
- (iii) For $T_{\text{dec}}^{\tilde{\tau}_R} < T_R$, the $\tilde{\tau}_R$ NLSP decouples as a weakly interacting massive particle before its decay into the axino LSP so that $Y_{\tilde{\tau}}$ is the thermal relic stau abundance, which does not depend on T_R .

The thermal relic stau abundance prior to decay can be calculated numerically. Its value depends on details of the SUSY model such as the mass splitting among the lightest Standard Model superpartners [36] or the left-right mixing of the stau NLSP [37, 38]. With the focus on the $\tilde{\tau}_R$ NLSP setting in this Letter, we consider three characteristic approximations:

$$Y_{\tilde{\tau}} \simeq \kappa \times 10^{-12} \left(\frac{m_{\tilde{\tau}}}{1 \text{ TeV}} \right), \quad \kappa = 0.7, 1.4, 2.8, \quad (8)$$

where κ accounts for typical differences in the annihilation processes of the sleptons. The value $\kappa = 0.7$ corresponds to the case with $m_{\tilde{B}} = 1.1 m_{\tilde{\tau}}$ and $m_{\tilde{\tau}} \ll m_{\tilde{e}, \tilde{\mu}}$, in which primordial stau annihilation involves only staus in

the initial state [36].⁴ The yield associated with $\kappa = 1.4$ is encountered if there is either additional stau–slepton coannihilation corresponding to $m_{\tilde{\tau}} \lesssim m_{\tilde{e}, \tilde{\mu}} < 1.1 m_{\tilde{\tau}}$ [36] or additional stau–bino coannihilation corresponding to $m_{\tilde{\tau}} \lesssim m_{\tilde{B}} < 1.1 m_{\tilde{\tau}}$ (cf. $Y_{\tilde{\tau}}$ contours close to the dashed line in the right panel of Fig. 3 in Ref. [39]). For an approximate degeneracy of $m_{\tilde{\tau}}$ with both $m_{\tilde{e}, \tilde{\mu}}$ and $m_{\tilde{B}}$, simultaneous stau–slepton–bino coannihilation can lead to an even larger $\kappa = 2.8$ in (8) (cf. $Y_{\tilde{\tau}}$ contours close to the dashed line in the left panel of Fig. 3 of Ref. [39]).

A non-thermally produced (NTP) axino density [1, 2, 3, 4]

$$\Omega_a^{\text{NTP}} h^2 = m_{\tilde{a}} Y_{\tilde{\tau}} s(T_0) h^2 / \rho_c \quad (9)$$

emerges since one axino LSP is emitted in each stau NLSP decay; $\rho_c/[s(T_0)h^2] = 3.6 \times 10^{-9} \text{ GeV}$ [15]. This density must not exceed the dark matter density [40]

$$\Omega_{\text{dm}}^{3\sigma} h^2 = 0.105_{-0.030}^{+0.021}, \quad (10)$$

where a nominal 3σ range is indicated and where $h = 0.73_{-0.03}^{+0.04}$ denotes the Hubble constant in units of $100 \text{ km Mpc}^{-1} \text{ s}^{-1}$. Additionally taking into account the thermally produced axino density Ω_a^{TP} [5, 8] and the axion density Ω_a , one obtains the dark matter constraint on the stau abundance prior to decay: $Y_{\tilde{\tau}} \leq Y_{\tilde{\tau}_{\text{dm}}}^{\text{max}}$ with

$$Y_{\tilde{\tau}_{\text{dm}}}^{\text{max}} = 4.5 \times 10^{-11} \left(\frac{\Omega_{\text{dm}} - \Omega_a^{\text{TP}} - \Omega_a}{0.126/h^2} \right) \left(\frac{10 \text{ GeV}}{m_{\tilde{a}}} \right). \quad (11)$$

For the most conservative case $\Omega_a^{\text{TP}} + \Omega_a \ll \Omega_{\text{dm}}$, we have illustrated the constraint on $m_{\tilde{a}}$ and $m_{\tilde{\tau}}$ obtained by confronting $Y_{\tilde{\tau}}$ with (11) already in Ref. [8].

For $\tau_{\tilde{\tau}} > 10^3 \text{ s}$, additional upper limits on $Y_{\tilde{\tau}_R^-} = Y_{\tilde{\tau}}/2$ occur since the negatively charged $\tilde{\tau}_R^-$ s can form (${}^4\text{He } \tilde{\tau}_R^-$) and (${}^8\text{Be } \tilde{\tau}_R^-$) bound states and can thereby catalyze primordial ${}^6\text{Li}$ and ${}^9\text{Be}$ production in excess of observationally inferred limits [12, 13, 14].⁵ In fact, the CBBN constraints on $m_{\tilde{a}}$ and $m_{\tilde{\tau}}$ obtained by confronting $Y_{\tilde{\tau}}$ with the CBBN-induced $\tau_{\tilde{\tau}}$ -dependent upper limits given in Ref. [14] have been presented for the first time in Ref. [8].

V. HADRONIC BBN CONSTRAINTS

Hadronic energy injection can affect the abundance of primordial deuterium substantially via hadrodisso- ciation of helium-4. In fact, we focus on the constraint on hadronic energy release imposed by the primordial abundance of D in this section. While additional constraints on late energy injection are imposed

⁴ The bino mass $m_{\tilde{B}} = 1.1 m_{\tilde{\tau}}$ considered in Ref. [36] represents a typical mass splitting in regions with $m_{\tilde{B}} > m_{\tilde{\tau}}$ encountered in scenarios such as the constrained MSSM (CMSSM).

⁵ We note that Ref. [41] has questioned the efficiency of the catalyzed production of ${}^9\text{Be}$ obtained in Refs. [13, 14], and announced a further clarification of this point in the future.

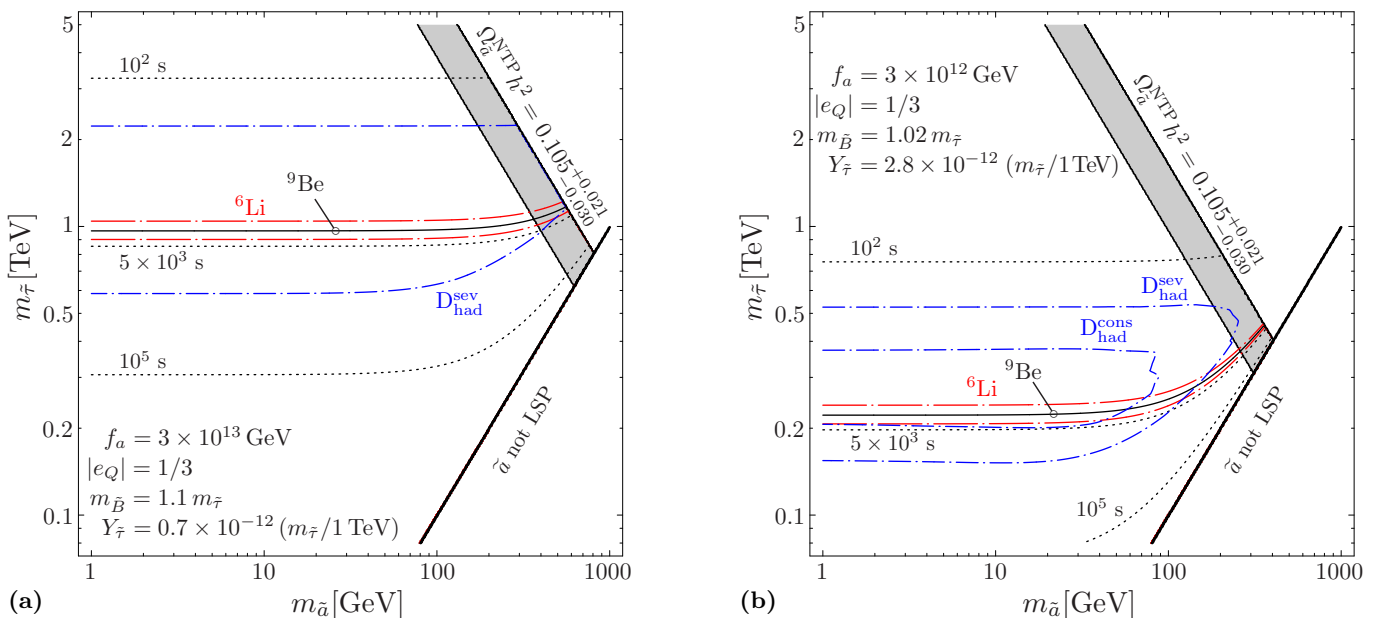


FIG. 3: Cosmological constraints on the masses of the \tilde{a} LSP and the $\tilde{\tau}_R$ NLSP for (a) $f_a = 3 \times 10^{13}$ GeV, $m_{\tilde{B}} = 1.1 m_{\tilde{\tau}}$, $Y_{\tilde{\tau}}$ given by (8) with $\kappa = 0.7$ and (b) $f_a = 3 \times 10^{12}$ GeV, $m_{\tilde{B}} = 1.02 m_{\tilde{\tau}}$, $Y_{\tilde{\tau}}$ given by (8) with $\kappa = 2.8$. In both panels, $|e_Q| = 1/3$ and $y = 1$. The hadronic BBN constraints associated with (13) and (14) disfavor the regions enclosed by the respective short-dash-dotted (blue) lines. The CBBN constraints associated with (15) and (16) disfavor the regions below the long-dash-dotted (red) and the solid lines. Contours of $\tau_{\tilde{\tau}} = 10^2$, 5×10^3 , and 10^5 s are shown by the dotted lines. On (above) the gray band, $\Omega_{\tilde{a}}^{\text{NTP}} \in \Omega_{\text{dm}}^{3\sigma}$ ($\Omega_{\tilde{a}}^{\text{NTP}} h^2 > 0.126$). The region with $m_{\tilde{a}} > m_{\tilde{\tau}}$ is not considered as we focus on the \tilde{a} LSP case.

by the primordial abundances of ${}^4\text{He}$, ${}^3\text{He}/\text{D}$, ${}^7\text{Li}$, and ${}^6\text{Li}/{}^7\text{Li}$ [23, 24, 25, 42, 43, 44, 45], the hadronic D constraint is the dominant one in the region allowed by the CBBN constraints, $\tau_{\tilde{\tau}_1} \lesssim 10^3$ s. This can be seen, e.g., in Figs. 38–41 of Ref. [23] and in Figs. 6–8 of Ref. [24]. Also the D constraint on electromagnetic energy injection is not considered in this section since it becomes relevant only for $\tau_{\tilde{\tau}_1} > 10^4$ s which is already disfavored by CBBN; see Sect. VI for details.

To derive the hadronic BBN constraint imposed by D, we use the τ_{NLSP} -dependent upper limits (95% CL) on

$$\xi_{\text{had}} \equiv \epsilon_{\text{had}} Y_{\text{NLSP}} \quad (12)$$

given in Fig. 9 of Ref. [29] as obtained in Ref. [23] for observationally inferred primordial D abundances of

$$\text{D}/\text{H}|_{\text{mean}} = (2.78_{-0.38}^{+0.44}) \times 10^{-5} \quad (\text{severe}), \quad (13)$$

$$\text{D}/\text{H}|_{\text{high}} = (3.98_{-0.67}^{+0.59}) \times 10^{-5} \quad (\text{conservative}). \quad (14)$$

Here $\tau_{\text{NLSP}} = \tau_{\tilde{\tau}}$, $Y_{\text{NLSP}} = Y_{\tilde{\tau}}$, and ϵ_{had} is given in (7). With the calculated ϵ_{had} , upper limits on $Y_{\tilde{\tau}}$ can be derived from the considered upper limits on ξ_{had} [46]: $Y_{\tilde{\tau}}^{\text{max}} = \xi_{\text{had}}^{\text{max}}/\epsilon_{\text{had}}$. By confronting $Y_{\tilde{\tau}}$ with $Y_{\tilde{\tau}}^{\text{max}}$, we then obtain the regions in the parameter space that are disfavored by the hadronic BBN constraints.

In Fig. 3 the obtained hadronic BBN constraints are shown by short-dash-dotted (blue) lines. The labels $\text{D}_{\text{had}}^{\text{sev}}$ and $\text{D}_{\text{had}}^{\text{cons}}$ indicate the constraints associated with (13) and (14), respectively. The regions enclosed by the corresponding lines are disfavored by an excess of D above

the respective observationally inferred abundance. The absence of a $\text{D}_{\text{had}}^{\text{cons}}$ line in panel (a) and the difference between the $\text{D}_{\text{had}}^{\text{sev}}$ and $\text{D}_{\text{had}}^{\text{cons}}$ lines in panel (b) indicate the sensitivity on the observationally inferred D abundance.

We also show the CBBN constraints associated with the observationally inferred limits on the respective primordial fractions of ${}^6\text{Li}$ [47, 48, 49] and ${}^9\text{Be}$ [14],

$${}^6\text{Li}/\text{H}|_{\text{obs}} \leq 10^{-11} - 10^{-10}, \quad (15)$$

$${}^9\text{Be}/\text{H}|_{\text{obs}} \leq 2.1 \times 10^{-13}, \quad (16)$$

as obtained by confronting $Y_{\tilde{\tau}_R}$ with the limits in Fig. 5 of Ref. [14]. The range (15) is indicated by pairs of long-dash-dotted (${}^6\text{Li}$, red) lines and (16) by solid (${}^9\text{Be}$) lines. The regions below those lines are disfavored by an excess of ${}^6\text{Li}$ and ${}^9\text{Be}$ above the respective limits. The region with $\Omega_{\tilde{a}}^{\text{NTP}} \in \Omega_{\text{dm}}^{3\sigma}$ is indicated by the gray band, where the region above that band is the one excluded by (11) in the conservative case with $\Omega_{\tilde{a}}^{\text{TP}} + \Omega_{\tilde{a}} \ll \Omega_{\text{dm}}$. The dotted lines are contours of $\tau_{\tilde{\tau}} = 10^2$, 5×10^3 , and 10^5 s.

For $|e_Q| = 1/3$ and $y = 1$, we consider $f_a = 3 \times 10^{13}$ GeV, $m_{\tilde{B}} = 1.1 m_{\tilde{\tau}}$, $Y_{\tilde{\tau}}$ given by (8) with $\kappa = 0.7$ in panel (a) and $f_a = 3 \times 10^{12}$ GeV, $m_{\tilde{B}} = 1.02 m_{\tilde{\tau}}$, $Y_{\tilde{\tau}}$ given by (8) with $\kappa = 2.8$ in panel (b). In both panels, one finds $m_{\tilde{\tau}}$ values disfavored by the hadronic BBN constraints that are significantly larger than the ones disfavored by the CBBN constraints. However, for $|e_Q| = 1/3$, $y = 1$, $m_{\tilde{B}} = 1.1 m_{\tilde{\tau}}$ and $\kappa = 0.7$, even the more restrictive ‘severe’ hadronic BBN constraint disappears for $f_a \lesssim 10^{13}$ GeV. In contrast, the CBBN constraints remain until $f_a \lesssim 10^{12}$ GeV—cf. Fig. 5(a)—given the limit

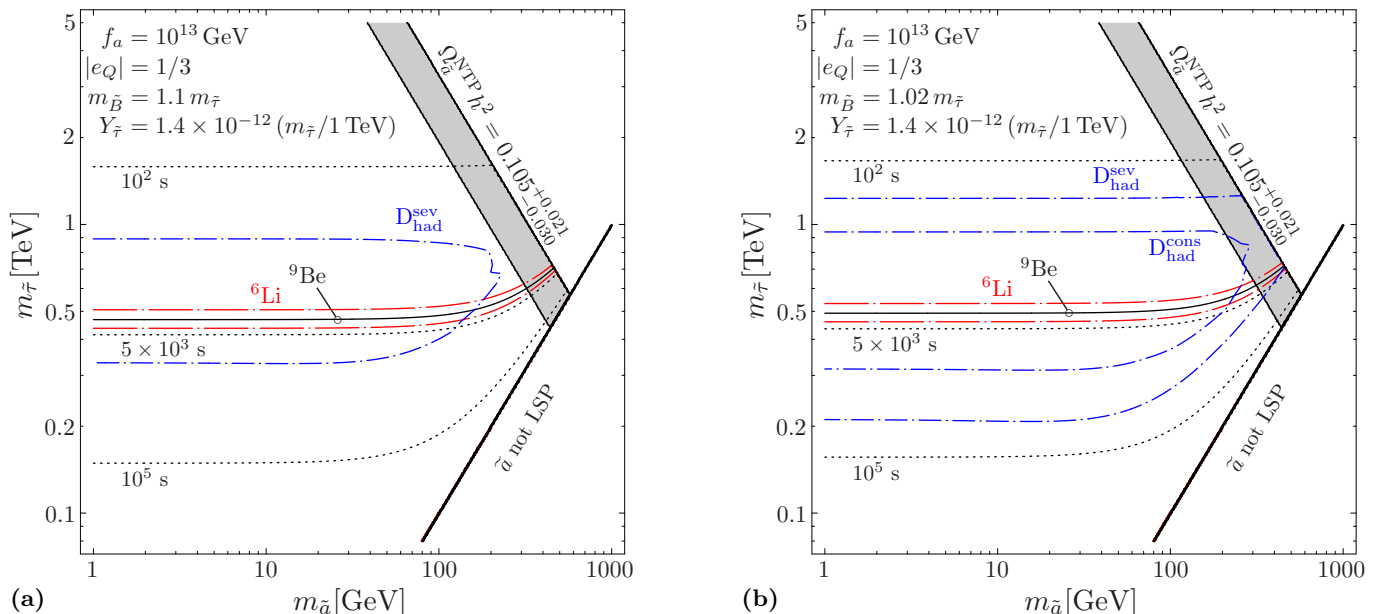


FIG. 4: Cosmological constraints on the masses of the \tilde{a} LSP and the $\tilde{\tau}_R$ NLSP for (a) $m_{\tilde{B}} = 1.1 m_{\tilde{\tau}}$ and (b) $m_{\tilde{B}} = 1.02 m_{\tilde{\tau}}$. In both panels, $f_a = 10^{13}$ GeV, $|e_Q| = 1/3$, $y = 1$, and $Y_{\tilde{\tau}}$ is given by (8) with $\kappa = 1.4$. The BBN constraints, the dark matter constraint, the $\tau_{\tilde{\tau}}$ contours, and the other regions are indicated as in Fig. 3.

$m_{\tilde{\tau}} \gtrsim 80$ GeV [15] from searches for long-lived staus at the Large Electron Positron (LEP) collider.

For $m_{\tilde{B}} = 1.02 m_{\tilde{\tau}}$ and $Y_{\tilde{\tau}}$ enhanced by stau–slepton–bino coannihilation such that $\kappa = 2.8$, Fig. 3(b) shows that ‘severe’ and ‘conservative’ hadronic BBN constraints are still encountered at $f_a = 3 \times 10^{12}$ GeV. This demonstrates the sensitivity of those constraints on the stau NLSP yield. In fact, the restrictive $D_{\text{had}}^{\text{sev}}$ constraint remains until $f_a \lesssim 10^{12}$ GeV for $\kappa = 2.8$; cf. Fig. 5(b).

In the latter case, more restrictive hadronic BBN constraints are encountered not only due to the enhanced yield but also due to the smaller bino mass which is associated with larger values of ϵ_{had} and thereby with more restrictive $Y_{\tilde{\tau}}^{\text{had}}^{\text{max}}$ values. Fig. 4 shows this more clearly for $f_a = 10^{13}$ GeV, $|e_Q| = 1/3$, $y = 1$, and $\kappa = 1.4$, where constraints and $\tau_{\tilde{\tau}}$ values are indicated as in Fig. 3. The two panels seen here only differ in the bino–stau mass ratio. The one on the left illustrates the case where we have $m_{\tilde{B}} = 1.1 m_{\tilde{\tau}}$ and stau–slepton coannihilation while the panel on the right illustrates the case where we have $m_{\tilde{B}} = 1.02 m_{\tilde{\tau}}$ and stau–bino coannihilation, where the different origins of coannihilation only serve to give the same $Y_{\tilde{\tau}}$ in the two cases. However, this change in bino–stau mass ratio alters the result sufficiently to produce much more restrictive D constraints in the latter case. We can trace this effect back to ϵ_{had} through Fig. 2, which illustrates the considerably higher curve for the case of $m_{\tilde{B}} = 1.02 m_{\tilde{\tau}}$ as compared to $m_{\tilde{B}} = 1.1 m_{\tilde{\tau}}$, with the same $m_{\tilde{a}}$, $m_{\tilde{\tau}}$, and f_a values (the top two curves in the plot). A thorough study of this and of other aspects of the hadronic BBN constraints will be presented in a forthcoming publication [46]. Our objective in the present Letter is (i) a first presentation of the hadronic

BBN constraints in the case with the axino LSP and a charged slepton NLSP and (ii) to demonstrate explicitly that they can be more restrictive than the associated CBBN constraints.

Before proceeding let us comment on the potential interplay between late energy injection and CBBN. The CBBN limits adopted from Ref. [14] have been derived for an abundance of D obtained with standard BBN. For an increased D abundance from hadrodissociation of ${}^4\text{He}$, CBBN of ${}^6\text{Li}$ and ${}^9\text{Be}$ becomes more efficient. This is evident for ${}^6\text{Li}$ since its catalysis proceeds via $({}^4\text{He} \tilde{\tau}_R^-) + \text{D} \rightarrow {}^6\text{Li} + \tilde{\tau}_R^-$ [12] and since the primordial abundance of D stays significantly below the one of ${}^4\text{He}$ at the relevant times (even for a maximum of observationally tolerable hadrodissociation of ${}^4\text{He}$); cf. Fig. 2.4 in Ref. [50]. An increased output of ${}^9\text{Be}$ results from the final step of its catalysis, $({}^8\text{Be} \tilde{\tau}_R^-) + n \rightarrow {}^9\text{Be} + \tilde{\tau}_R^-$ [13, 14], which becomes more efficient since an enhanced abundance of D increases the number of neutrons n at the relevant times [51]; cf. Fig. 4 in Ref. [14]. Moreover, the debris of hadrodissociated ${}^4\text{He}$ can hit ambient ${}^4\text{He}$ and thereby fuse additional ${}^6\text{Li}$ [23, 24, 44]. The interplay of late energy injection and CBBN will thus lead to constraints that can only be stronger than the ones presented in this Letter. Aiming at conservative limits, this allows us to neglect those intricacies which will have to be faced in future refinements of the presented constraints.

VI. BBN CONSTRAINTS ON THE PQ SCALE

In this section we show that the BBN constraints associated with hadronic and electromagnetic energy release

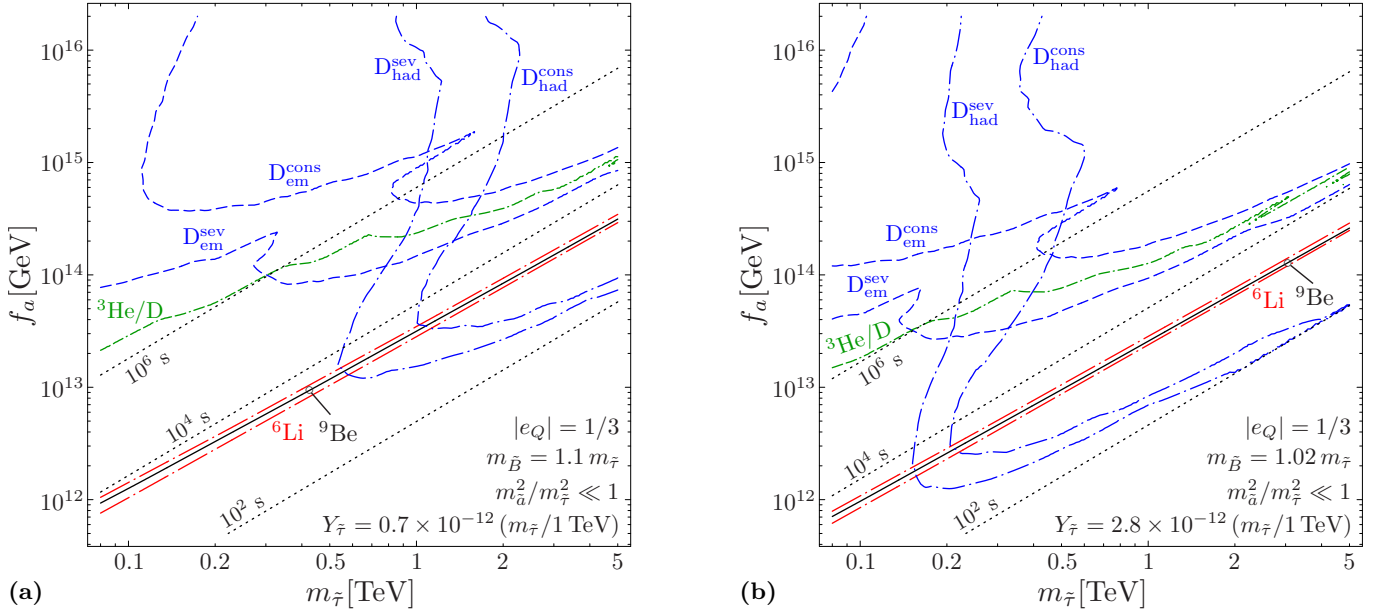


FIG. 5: BBN constraints on the PQ scale f_a , shown for (a) $m_{\tilde{B}} = 1.1 m_{\tilde{\tau}}$, $Y_{\tilde{\tau}}$ given by (8) with $\kappa = 0.7$ and (b) $m_{\tilde{B}} = 1.02 m_{\tilde{\tau}}$, $Y_{\tilde{\tau}}$ given by (8) with $\kappa = 2.8$. In both panels, $m_{\tilde{a}}^2/m_{\tilde{\tau}}^2 \ll 1$, $|e_Q| = 1/3$, and $y = 1$. The hadronic BBN constraints associated with (13) and (14) disfavor the regions in the upper right-hand corner enclosed by the respective short-dash-dotted (blue) lines. Electromagnetic BBN constraints associated with D disfavor the upper regions enclosed by the respective dashed (blue) lines and the ones associated with ${}^3\text{He}/\text{D}$ the region above the double-dash-dotted (green) line. The regions above the long-dash-dotted (red) and the solid lines are disfavored by the CBBN constraints associated with (15) and (16). Contours of $\tau_{\tilde{\tau}} = 10^2$, 10^4 , and 10^6 s are shown by the dotted lines.

impose new upper limits on the PQ scale f_a . In agreement with the results of the previous section, we find that those limits can be substantially more restrictive than the ones imposed by the CBBN constraints [8].

Fig. 5 presents the new f_a limits together with the CBBN limits for $m_{\tilde{a}}^2/m_{\tilde{\tau}}^2 \ll 1$, $|e_Q| = 1/3$, and $y = 1$. In panel (a) we have the generic case of $m_{\tilde{B}} = 1.1 m_{\tilde{\tau}}$ and $Y_{\tilde{\tau}}$ given by (8) with $\kappa = 0.7$ while in panel (b) we have $m_{\tilde{B}} = 1.02 m_{\tilde{\tau}}$ and $\kappa = 2.8$ representing the case with simultaneous stau–slepton–bino coannihilation. Contours of $\tau_{\tilde{\tau}} = 10^2$, 10^4 , and 10^6 s are shown by the dotted lines. Above the long-dash-dotted (red) and the solid lines, CBBN of ${}^6\text{Li}$ and ${}^9\text{Be}$ is in excess of the respective limits (15) and (16). The new hadronic BBN constraints associated with (13) and (14) disfavor the regions in the upper right-hand corner enclosed by the respective short-dash-dotted (blue) lines. Note that those constraints are provided only for $\tau_{\tilde{\tau}} \geq 100$ s since we have not considered the typically milder limits associated with proton–neutron interconversion processes [26] which become relevant for smaller $\tau_{\tilde{\tau}}$ [23, 24, 25]. Nevertheless, the hadronic BBN constraints place limits on the PQ scale f_a that become clearly more restrictive than the CBBN-induced limits towards large $m_{\tilde{\tau}}$ and/or large $Y_{\tilde{\tau}}$. In fact, the hadronic BBN constraint on f_a can be the dominant one already in a mass range, $m_{\tilde{\tau}} < 1$ TeV, that is promising for a discovery of a long-lived stau at the LHC.

While the above sets of BBN constraints correspond to

the ones shown in the previous section (cf. Fig. 3), we also indicate in Fig. 5 the electromagnetic BBN constraints imposed by primordial D and ${}^3\text{He}/\text{D}$. Our derivation of the electromagnetic BBN constraints proceeds as outlined for the hadronic ones in Sect. V but relies on the conservative ϵ_{em} (6) and on upper limits on $\xi_{\text{em}} \equiv \epsilon_{\text{em}} Y_{\tilde{\tau}}$. Accordingly, we obtain the shown $D_{\text{em}}^{\text{sew}}$ and ${}^3\text{He}/\text{D}$ constraints from the respective limits given in Fig. 42 of Ref. [23] and the $D_{\text{em}}^{\text{cons}}$ constraint from the respective limit given in Fig. 6 of Ref. [47]. Those $D_{\text{em}}^{\text{sew/cons}}$ and ${}^3\text{He}/\text{D}$ constraints disfavor the upper regions enclosed by the respective dashed (blue) lines and the regions above the double-dash-dotted (green) lines in Fig. 5.

Fig. 5 shows that the electromagnetic BBN constraints appear only for $\tau_{\tilde{\tau}_1} > 10^4$ s thereby excluding regions already disfavored by CBBN. Nevertheless, they support the finding that, e.g., values of the PQ scale at the scale of grand unification, $f_a \sim 10^{16}$ GeV, will be in conflict with successful BBN in the considered scenarios once a long-lived charged slepton is observed at the LHC.

Before closing let us discuss the robustness of the shown f_a limits and address important sensitivities:

- By considering $m_{\tilde{a}}^2/m_{\tilde{\tau}}^2 \ll 1$, the CBBN-imposed f_a limits are conservative limits. Those constraints become more restrictive for $m_{\tilde{a}} \rightarrow m_{\tilde{\tau}}$. This is different for constraints associated with late energy injection, where any bound can be evaded for a finely tuned $m_{\tilde{a}}-m_{\tilde{\tau}}$ degeneracy leading to $\epsilon_{\text{had/em}} \rightarrow 0$.

- The f_a limits are sensitive to $Y_{\tilde{\tau}}$. In settings with a sizable left-right stau mixing, an exceptionally small $Y_{\tilde{\tau}}$ is possible such that even the CBBN constraints may be respected [37, 38].
- The f_a limits depend on the quantum numbers of the heavy KSVZ fields. While $\epsilon_{\text{had/em}}$ are independent of e_Q , $\tau_{\tilde{\tau}} \propto 1/e_Q^4$. The f_a limits can thus be relaxed, e.g., by one order of magnitude for $e_Q = 1$.
- The CBBN and hadronic BBN constraints in the case of the \tilde{e}_R or $\tilde{\mu}_R$ NLSP are identical to the ones shown. The electromagnetic BBN constraints however will be more restrictive in the \tilde{e}_R NLSP case since all of the electron energy E_e released in the \tilde{e}_R NLSP decay will contribute: $\epsilon_{\text{em}} = E_e$.

VII. CONCLUSION

For axino LSP scenarios with a long-lived charged slepton NLSP, we have studied BBN constraints associated

with hadronic and electromagnetic energy release. While the region with $f_a \lesssim 10^{12}$ GeV is typically not affected, those constraints become significant for larger f_a such that models with f_a towards the grand unification scale are disfavored. The new BBN constraints on f_a can be more restrictive than the recently obtained CBBN constraints [8]. This further tightens the upper limits on the reheating temperature discussed in Ref. [8] which are relevant for models of inflation and baryogenesis.

Acknowledgments

N.T. would like to thank the Max Planck Institute for Physics for their kind hospitality during parts of this work. This research was partially supported by the Cluster of Excellence ‘Origin and Structure of the Universe’ and by the Swiss National Science Foundation (SNF).

-
- [1] S.A. Bonometto, F. Gabbiani, A. Masiero, Phys. Rev. **D49**, 3918 (1994), [hep-ph/9305237](#)
- [2] L. Covi, J.E. Kim, L. Roszkowski, Phys. Rev. Lett. **82**, 4180 (1999), [hep-ph/9905212](#)
- [3] L. Covi, H.B. Kim, J.E. Kim, L. Roszkowski, JHEP **05**, 033 (2001), [hep-ph/0101009](#)
- [4] L. Covi, L. Roszkowski, R. Ruiz de Austri, M. Small, JHEP **06**, 003 (2004), [hep-ph/0402240](#)
- [5] A. Brandenburg, F.D. Steffen, JCAP **0408**, 008 (2004), [hep-ph/0405158](#)
- [6] F.D. Steffen, Eur. Phys. J. **C59**, 557 (2009), [0811.3347](#)
- [7] H. Baer, M. Haider, S. Kraml, S. Sekmen, H. Summy, JCAP **0902**, 002 (2009), [0812.2693](#)
- [8] A. Freitas, F.D. Steffen, N. Tajuddin, D. Wyler, Phys. Lett. **B679**, 270 (2009), [0904.3218](#)
- [9] K.Y. Choi, L. Roszkowski, R. Ruiz de Austri, JHEP **04**, 016 (2008), [0710.3349](#)
- [10] M. Kawasaki, K. Nakayama, M. Senami, JCAP **0803**, 009 (2008), [0711.3083](#)
- [11] H. Baer, A.D. Box, H. Summy (2009), [0906.2595](#)
- [12] M. Pospelov, Phys. Rev. Lett. **98**, 231301 (2007), [hep-ph/0605215](#)
- [13] M. Pospelov (2007), [0712.0647](#)
- [14] M. Pospelov, J. Pradler, F.D. Steffen, JCAP **0811**, 020 (2008), [0807.4287](#)
- [15] C. Amsler et al. (Particle Data Group), Phys. Lett. **B667**, 1 (2008)
- [16] P. Sikivie, Lect. Notes Phys. **741**, 19 (2008), [astro-ph/0610440](#)
- [17] G.G. Raffelt, Lect. Notes Phys. **741**, 51 (2008), [hep-ph/0611350](#)
- [18] J.E. Kim, Phys. Rev. Lett. **43**, 103 (1979)
- [19] M.A. Shifman, A.I. Vainshtein, V.I. Zakharov, Nucl. Phys. **B166**, 493 (1980)
- [20] J.E. Kim, Phys. Lett. **B136**, 378 (1984)
- [21] S. Schilling, *Two-Loop Techniques in Rare Decays* (2005), PhD Thesis, University of Zuerich
- [22] A. Brandenburg, L. Covi, K. Hamaguchi, L. Roszkowski, F.D. Steffen, Phys. Lett. **B617**, 99 (2005), [hep-ph/0501287](#)
- [23] M. Kawasaki, K. Kohri, T. Moroi, Phys. Rev. **D71**, 083502 (2005), [astro-ph/0408426](#)
- [24] K. Jedamzik, Phys. Rev. **D74**, 103509 (2006), [hep-ph/0604251](#)
- [25] R.H. Cyburt et al. (2009), [0907.5003](#)
- [26] M.H. Reno, D. Seckel, Phys. Rev. **D37**, 3441 (1988)
- [27] M. Kawasaki, K. Kohri, T. Moroi, A. Yotsuyanagi, Phys. Rev. **D78**, 065011 (2008), [0804.3745](#)
- [28] J.L. Feng, A. Rajaraman, F. Takayama, Phys. Rev. **D68**, 063504 (2003), [hep-ph/0306024](#)
- [29] F.D. Steffen, JCAP **0609**, 001 (2006), [hep-ph/0605306](#)
- [30] K. Kohri, T. Moroi, A. Yotsuyanagi, Phys. Rev. **D73**, 123511 (2006), [hep-ph/0507245](#)
- [31] S. Bailly, K. Jedamzik, G. Moulata, Phys. Rev. **D80**, 063509 (2009), [0812.0788](#)
- [32] J.E. Kim, Phys. Rev. Lett. **67**, 3465 (1991)
- [33] D.H. Lyth, Phys. Rev. **D48**, 4523 (1993), [hep-ph/9306293](#)
- [34] S. Chang, H.B. Kim, Phys. Rev. Lett. **77**, 591 (1996), [hep-ph/9604222](#)
- [35] M. Hashimoto, K.I. Izawa, M. Yamaguchi, T. Yanagida, Phys. Lett. **B437**, 44 (1998), [hep-ph/9803263](#)
- [36] T. Asaka, K. Hamaguchi, K. Suzuki, Phys. Lett. **B490**, 136 (2000), [hep-ph/0005136](#)
- [37] M. Ratz, K. Schmidt-Hoberg, M.W. Winkler, JCAP **0810**, 026 (2008), [0808.0829](#)
- [38] J. Pradler, F.D. Steffen, Nucl. Phys. **B809**, 318 (2009), [0808.2462](#)
- [39] J. Pradler, F.D. Steffen, Phys. Lett. **B648**, 224 (2007), [hep-ph/0612291](#)
- [40] D.N. Spergel et al. (WMAP), Astrophys. J. Suppl. **170**, 377 (2007), [astro-ph/0603449](#)

- [41] M. Kamimura, Y. Kino, E. Hiyama, Prog. Theor. Phys. **121**, 1059 (2009), 0809.4772
- [42] G. Sigl, K. Jedamzik, D.N. Schramm, V.S. Berezinsky, Phys. Rev. **D52**, 6682 (1995), astro-ph/9503094
- [43] K. Jedamzik, Phys. Rev. Lett. **84**, 3248 (2000), astro-ph/9909445
- [44] K. Jedamzik, Phys. Rev. **D70**, 063524 (2004), astro-ph/0402344
- [45] R.H. Cyburt, J.R. Ellis, B.D. Fields, K.A. Olive, V.C. Spanos, JCAP **0611**, 014 (2006), astro-ph/0608562
- [46] A. Freitas, F.D. Steffen, N. Tajuddin, D. Wyler (2009), in preparation
- [47] R.H. Cyburt, J.R. Ellis, B.D. Fields, K.A. Olive, Phys. Rev. **D67**, 103521 (2003), astro-ph/0211258
- [48] M. Asplund, D.L. Lambert, P.E. Nissen, F. Primas, V.V. Smith, Astrophys. J. **644**, 229 (2006), astro-ph/0510636
- [49] K. Jedamzik, JCAP **0803**, 008 (2008), 0710.5153v2
- [50] J. Pradler, *The long-lived stau as a thermal relic* (2009), PhD Thesis, Technical University Munich, 0909.3429
- [51] V.F. Mukhanov, Int. J. Theor. Phys. **43**, 669 (2004), astro-ph/0303073